XLVI CILAMCE
VITÓRIA - ES - BRAZIL - 2025
XLVI IBERO-LATIN AMERICAN CONGRESS ON COMPUTATIONAL METHODS IN ENGINEERING

A formulation based on Flory's decomposition for thermomechanical analysis of thermoelastic solids

Eduardo Yuiti Hayashi[1], Humberto Breves Coda[1]

[1]*Dept. of Structural Engineering, São Carlos School of Engineering, University of São Paulo*
Av. Trabalhador São Carlense, 400, Parque Arnold Schimidt,13566-590, São Paulo/São Carlos, Brazil
yuitihayashi@gmail.com, hbcoda@sc.usp.br

Abstract. This study presents an alternative thermoelastic constitutive model developed using Flory's multiplicative decomposition of the deformation gradient tensor into volumetric and isochoric components. The model combines the Rivlin–Saunders and Hartmann–Neff constitutive formulations, making it suitable for large strain analysis. In themomechanical analysis it means that there should not occur material annihilation with finite temperature change, which usually occurs when no special attention is given to the constitutive model. In this paper the mechanical analysis was performed numerically using the position-based Finite Element Method, which intrinsically accounts for geometric nonlinearities. Thermal analysis was also conducted using the Finite Element Method, formulated from the transient heat conduction equation. Thermomechanical coupling was solved numerically using a partitioned explicit approach. In order to allow comparisons, and to show the material annihilation issue, the small to moderate strain Saint-Venant–Kirchhoff-based thermoelastic model was also implemented.

Keywords: Thermoelasticity, Flory's decomposition, Rivlin-Saunders, Hartmann-Neff, Finite Element Method.

1 Introduction

In several engineering fields, thermomechanical analysis is crucial for the analysis of materials and structures, due to the importance of considering the degradation of mechanical properties and behavior under significant thermal loads. In these situations, larger displacements and strains of bodies are frequently observed, exhibiting an intrinsic geometric and physical nonlinear behavior. Given the importance of the constitutive model for the proper simulation of material behavior, an alternative thermoelastic constitutive model based on Flory's decomposition [1] and Rivlin-Saunders [2] and Hartmann-Neff [3] hyperelastic constitutive models was developed.

To this end, a computational code was developed employing the Finite Element Method (FEM) as the primary numerical tool, using the formulations presented by Hayashi [4]. The thermal analysis was conducted using a Fourier's law FEM formulation, while the mechanical analysis adopted a position-based FEM approach [5]. The temperature-strain relation is the original contribution related to thermomechanical coupling of this study, as it enables the volumetric coupling in a realistic way for large strain situations.

In this article, tensors are represented using symbolic notation. In general, scalars are denoted by letters (a), first-order tensors (vectors) by letters with an overhead arrow ($\vec{a}$) and second-order tensors by bold capital letters ($\boldsymbol{A}$). Single contractions are indicated by a single dot ($\cdot$) between two tensors and double contractions are denoted by a double dot ($:$), while tensor products are denoted by tensor product symbol ($\otimes$).

2 Position-based Finite Element Method

The position-based Finite Element Method, as introduced by Bonet et al. [6] and Coda [7], is a numerical technique for discretizing domains to obtain approximate solutions of nonlinear equations derived from

mechanical potential energy and employs a geometrically exact approach based on positions. The alternative formulation uses the current nodal positions as the primary unknowns instead of displacements and adopts a total Lagrangian framework, referencing the current configuration to the initial one. The following sections provide a summary of the position-based FEM, and further details can be found in the works of Coda [7], Ramos et al. [8], Kishino et al. [9] and Carvalho et al. [10].

2.1 Saint-Venant-Kirchhoff constitutive law

To describe a geometrically nonlinear formulation, an objective strain measure is required – one that results in zero strain under rigid body translations and rotations. The Green–Lagrange strain tensor ($\mathbb{E}$) satisfies this requirement, it is an objective, Lagrangian measure defined by the following expression:

$$\mathbb{E} = \frac{1}{2}(\boldsymbol{A}^t \cdot \boldsymbol{A} - \boldsymbol{I}) = \frac{1}{2}(\boldsymbol{C} - \boldsymbol{I}) \tag{1}$$

where $\boldsymbol{C}$ is the right Cauchy-Green stretch tensor and $\boldsymbol{I}$ is the second-order identity tensor.

The Saint-Venant-Kirchhoff constitutive relation is the first model used in this study, and it is suitable for large displacements and small or moderate strains. This model defines a linear relationship between the second Piola-Kirchhoff stress tensor ($\boldsymbol{S}$) and the Green-Lagrange strain tensor. Thus, the specific strain energy (Ψ) can be expressed as:

$$\Psi = \frac{1}{2}\mathbb{E} : \mathfrak{C} : \mathbb{E} = \frac{1}{2}\boldsymbol{S} : \mathbb{E} \tag{2}$$

where $\mathfrak{C}$ is the fourth-order elastic constitutive tensor.

2.2 Flory's decomposition and Rivlin-Saunders-Hartmann-Neff constitutive law

Flory's decomposition splits the specific strain energy into volumetric and isochoric components, based on the multiplicative decomposition of the deformation gradient ($\boldsymbol{A}$) into volumetric ($\widehat{\boldsymbol{A}} = J^{1/3}\,\boldsymbol{I}$) and isochoric ($\overline{\boldsymbol{A}} = J^{-1/3}\,\boldsymbol{A}$) parts:

$$\boldsymbol{A} = \widehat{\boldsymbol{A}} \cdot \overline{\boldsymbol{A}} = \left(J^{1/3}\,\boldsymbol{I}\right) \cdot \left(J^{-1/3}\,\boldsymbol{A}\right) \tag{3}$$

where J is the Jacobian.

Consequently, the multiplicative decomposition of the right Cauchy-Green stretch tensor can be expressed in terms of its isochoric $\overline{\boldsymbol{C}} = J^{-2/3}\,\boldsymbol{C}$ and volumetric $\widehat{\boldsymbol{C}} = J^{2/3}\,\boldsymbol{I}$ components:

$$\boldsymbol{C} = \widehat{\boldsymbol{C}} \cdot \overline{\boldsymbol{C}} = \overline{\boldsymbol{C}} \cdot \widehat{\boldsymbol{C}}. \tag{4}$$

It is noted that $det\left(\widehat{\boldsymbol{C}}\right) = J^2$ and $det(\overline{\boldsymbol{C}}) = 1$ with the Jacobian having the physical meaning of volumetric stretch. Therefore, it can be concluded that $\widehat{\boldsymbol{C}}$ and $\overline{\boldsymbol{C}}$ correspond to the volumetric and isochoric components, respectively, of the right Cauchy-Green stretch tensor.

In this way, it becomes possible to perform the additive decomposition of the specific strain energy into volumetric (Ψ^{vol}) and isochoric (Ψ^{isoc}) components. For isotropic materials, the isochoric part can be expressed separately as a function of the first and second principal invariants ($\bar{I}_1$ and $\bar{I}_2$) of $\overline{\boldsymbol{C}}$. In this work, the isochoric and volumetric components of the specific strain energy are described by the constitutive models of Rivlin-Saunders and Hartmann-Neff, respectively. Under small strains, these nonlinear constitutive laws must behave similarly to the Saint-Venant–Kirchhoff model. Considering this condition, the isochoric and volumetric components of the specific strain energy can be expressed as follows:

$$\Psi = \Psi^{vol}(J) + \Psi^{isoc1}(\bar{I}_1) + \Psi^{isoc2}(\bar{I}_2) = \frac{K}{8n^2}(J^{2n} + J^{-2n} - 2) + \frac{G}{4}(\bar{I}_1 - 3) + \frac{G}{4}(\bar{I}_2 - 3)\,. \tag{5}$$

where G is the shear modulus, K is the bulk modulus and n is a constant that controls the volumetric stiffness.

2.3 Principle of Stationarity of Mechanical Energy and solution strategy

According to the Principle of Stationarity of Mechanical Energy, a body is in mechanical equilibrium when the first variation of its mechanical energy (Π) – defined as the sum of the work of external forces ($\mathbb{P}$), internal strain energy ($\mathbb{U}$), and kinetic energy ($\mathbb{K}$) – is zero.

In the position-based FEM, current nodal positions are treated as unknowns, resulting in a set of nonlinear equations solved using the Newton-Raphson method [11]. Although they are the unknowns of the problem, their values are known in trial form throughout the entire analysis. This process generates an imbalance among the internal $\vec{F}^{int}$, external $\vec{F}^{ext}$, and inertial $\vec{F}^{iner}$ force vectors, represented by the mechanical residual vector $\vec{g}$:

$$\vec{g} = \frac{\partial \Pi}{\partial \vec{Y}} = \frac{\partial \mathbb{U}}{\partial \vec{Y}} + \frac{\partial \mathbb{P}}{\partial \vec{Y}} + \frac{\partial \mathbb{K}}{\partial \vec{Y}} = \vec{F}^{int} - \vec{F}^{ext} + \vec{F}^{iner} \neq \vec{0}\,. \tag{6}$$

The Newton–Raphson method determines the current configuration by minimizing $\vec{g}$ to zero. Assuming that the components of $\vec{g}$ are continuous functions in the vicinity of the solution and starting from a trial solution $\vec{Y}^0$ close to the exact solution, $\vec{g}$ can be approximated by first-order Taylor series expansion:

$$\vec{g}(\vec{Y}) = \vec{g}(\vec{Y}^0) + \left.\frac{\partial \vec{g}}{\partial \vec{Y}}\right|_{\vec{Y}^0} \Delta\vec{Y} \approx \vec{0} \;\rightarrow\; \left.\frac{\partial \vec{g}}{\partial \vec{Y}}\right|_{\vec{Y}^0} \Delta\vec{Y} = -\vec{g}(\vec{Y}^0) \;\rightarrow\; \boldsymbol{H}\cdot\Delta\vec{Y} = -\vec{g}(\vec{Y}^0) \tag{7}$$

where $\Delta\vec{Y}$ is the current nodal position correction vector and $\boldsymbol{H}$ is the Hessian or tangent stiffness matrix evaluated at the trial position.

The solution is refined iteratively by updating $\vec{Y} = \vec{Y} + \Delta\vec{Y}$ until the correction falls below a predefined tolerance (tol), with the stopping criterion expressed as $\|\Delta\vec{Y}\|/\|\vec{X}\| < tol$, where $\|\vec{X}\|$ is the Euclidean norm of the initial nodal position vector.

3 Finite Element Method for Thermal Field

Similarly to the mechanical field, the thermal field was solved numerically using the FEM, which in this case was based on temperatures and formulated using a total Lagrangian description. The following sections provide a summary of the temperature-based FEM, and further details can be found in the works of Hayashi [4], Rigobello et al. [12] and Salomão and Carrazedo [13].

3.1 Heat conduction equation for FEM

First, the heat conduction equation is considered in its local form:

$$\boldsymbol{\nabla}_0 \cdot \vec{q}_0 + \rho_0 c\dot{\theta} - r = 0\,. \tag{8}$$

where $\boldsymbol{\nabla}_0$ is the gradient with respect to the initial configuration, $\vec{q}_0$ is the heat flux in the initial configuration, ρ_0 is the initial mass density, c is the specific heat, $\dot{\theta}$ is the time rate of temperature change and r is the internal heat absorbed or released per unit initial volume.

Equation (8) can be expressed in its global variational form by multiplying it by a weighting function $\delta\theta$ and integrating over the initial volume. By incorporating the convection boundary condition to account for heat exchange with the environment via Newton's law of cooling, applying Fourier's law to describe heat flux, and considering the arbitrariness of $\delta\theta$, along with using the backward Euler method for time integration and interpolating the temperature field within the finite element formulation, the heat conduction equation can be reformulated into a suitable form for FEM implementation after appropriate mathematical manipulations:

$$\begin{aligned}\left(\int_{V_0} \boldsymbol{\nabla}_0\vec{\phi}\cdot\boldsymbol{K}_0\cdot\boldsymbol{\nabla}_0\vec{\phi}\,dV_0 + \int_{A_c} h^c\vec{\phi}\otimes\vec{\phi}\,dA_0 + \Delta t^{-1}\int_{V_0}\rho_0 c\vec{\phi}\otimes\vec{\phi}\,dV_0\right)\cdot\vec{\theta}_{s+1} \\ = \int_{V_0} r\vec{\phi}\,dV_0 - \int_{A_0}\bar{q}_0\vec{\phi}\,dA_0 + \int_{A_c} h^c\theta_\infty\vec{\phi}\,dA_0 + \left(\Delta t^{-1}\int_{V_0}\rho c\vec{\phi}\otimes\vec{\phi}\,dV_0\right)\cdot\vec{\theta}_s\end{aligned} \tag{9}$$

where $\vec{\theta}_{s+1}$ is the vector of nodal temperatures of current time step, $\vec{\theta}_s$ is the vector of nodal temperatures of previous time step, $\vec{\phi}$ is the vector of shape functions, $\boldsymbol{K}_0$ is the Lagrangian thermal conductivity matrix, $\bar{q}_0$ is the prescribed heat flux on the initial body boundary, h^c is the convection heat transfer coefficient, θ_∞ is the ambient temperature, Δt is the time step, A_0 is the initial surface area of the solid, A_c is the surface area of the solid subjected to convective heat flux and V_0 is the initial volume of the solid.

The solution strategy for the thermal problem is similar to that described for the mechanical problem, employing the Newton-Raphson method to solve the system of equations, with $\vec{\theta}_{s+1}$ being the vector of unknown nodal temperatures at the current time step for the thermal problem.

4 Thermomechanical Coupling

The thermomechanical coupling was solved numerically using a partitioned explicit approach (uncoupled thermomechanical model). In this strategy, information exchange occurs only once per time step and the thermal and mechanical problems are solved separately. Information is exchanged between the two physical fields explicitly, a strategy also known as weak coupling. At each time step, the thermal problem is first solved using the positions from the previous time step, followed by solving the mechanical problem using the temperatures calculated earlier in the current time step, before advancing to the next time step.

4.1 Thermomechanical coupling for Saint-Venant-Kirchhoff constitutive model

The Saint-Venant–Kirchhoff thermoelastic model is suitable for small to moderate strain regimes and is not suitable for large strain problems. The thermal strain ($\mathbb{E}^\theta$) is introduced as an imposed strain due to temperature change and is defined as:

$$\mathbb{E}^\theta = \alpha_l\left(\theta - \theta^{\{0\}}\right)\boldsymbol{I} = \alpha_l \Delta\theta\, \boldsymbol{I} \tag{10}$$

where α_l is the linear coefficient of thermal expansion, $\theta^{\{0\}}$ is the initial reference temperature of the body and $\Delta\theta$ is the temperature change.

After solving the thermal field, the elastic problem considers both the elastic stress/strain and the thermally induced stress/strain. Thus, the stress induced by thermal effects (which consists solely of the volumetric component) is subtracted from the total elastic stress:

$$\boldsymbol{S}^{TE} = \boldsymbol{S}^{elast} - \boldsymbol{S}^{therm} = \boldsymbol{S}^{elast} - K\varepsilon_v^\theta \boldsymbol{I} = \boldsymbol{S}^{elast} - K\, tr\left(\mathbb{E}^\theta\right)\boldsymbol{I} \tag{11}$$

where ε_v^θ is the volumetric strain induced by the temperature change when small strains are considered.

4.2 Thermomechanical coupling for Rivlin-Saunders-Hartmann-Neff constitutive model

This section presents the thermoelastic formulations related to the Rivlin–Saunders–Hartmann–Neff model, which is suitable for large strain problems. First, the expression for the variation of the volumetric thermoelastic energy is written as $(\delta\Psi^{vol})^{TE} = (\boldsymbol{S}^{vol})^{TE} : \delta\mathbb{E}$, where $(\boldsymbol{S}^{vol})^{TE}$ is the volumetric thermoelastic second Piola–Kirchhoff stress and $\delta\mathbb{E}$ is the variation of the Green-Lagrange strain tensor.

Based on the correspondence between the Cauchy hydrostatic stress and the volumetric component of the second Piola–Kirchhoff stress [14], the thermoelastic stress is calculated as follows:

$$(\delta\Psi^{vol})^{TE} = \left[s^{elast} - s^\theta\right]\delta J = \left[s^{elast} - s^\theta\right]\frac{\partial J}{\partial \mathbb{E}} : \delta\mathbb{E} = \left[s^{elast} - s^\theta\right]\mathfrak{C}^{vol} : \delta\mathbb{E} \tag{12}$$

where s^{elast} is the scalar value of the elastic hydrostatic stress, s^θ is the scalar value of the hydrostatic stress induced by the thermal field, and $\mathfrak{C}^{vol}$ is the Lagrangian hydrostatic strain direction. s^{elast} and s^θ are given by:

$$s^{elast} = K\varepsilon_v^{elast} = 0.25Kn^{-1}\left[J^{2n-1} - J^{-(2n+1)}\right], \tag{13}$$

$$s^\theta = K\varepsilon_v^\theta = K\alpha_v\left(\theta - \theta^{\{0\}}\right) = K\alpha_v\Delta\theta \tag{14}$$

with ε_v^{elast} and ε_v^{θ} being, respectively, the elastic volumetric strain assumed in the Hartmann–Neff constitutive model and the thermal volumetric strain, while α_v is the volumetric thermal expansion coefficient.

Thus, by analogy with the linear elastic problem, eq.(12) can be rewritten as:

$$(\boldsymbol{S}^{vol})^{TE} = K\left(\varepsilon_v^{elast} - \varepsilon_v^{\theta}\right)\mathbb{E}^{vol} = K\varepsilon_v^{elast}\mathbb{E}^{vol} - K\varepsilon_v^{\theta}\mathbb{E}^{vol} \,. \tag{15}$$

5 Numerical Example 1 – Thermoelastic cube

This numerical example aims to verify and compare the Saint-Venant–Kirchhoff and Rivlin–Saunders–Hartmann–Neff thermoelastic models in large volumetric strain problems. A unit-dimension thermoelastic cube supported on three frictionless surfaces was considered, with displacement constraints applied in the x, y, and z directions on the faces $x = 0$, $y = 0$, and $z = 0$, respectively.

Initially, the consistency of both models under small strains was verified, where identical results are expected. A linear thermal expansion coefficient of $\alpha_l = 10^{-6}\mathrm{K}^{-1}$ ($\alpha_v = 3\alpha_l$) and a temperature change of $\Delta\theta = 10$ K were adopted, applied from an initial undeformed and undisplaced configuration (Fig. 1). Under these conditions, both models produced displacements of 10^{-5}m on the three free faces, in agreement with the analytical length variation value ($\Delta l = \alpha_l \Delta\theta l_0 = 10^{-5}$m).

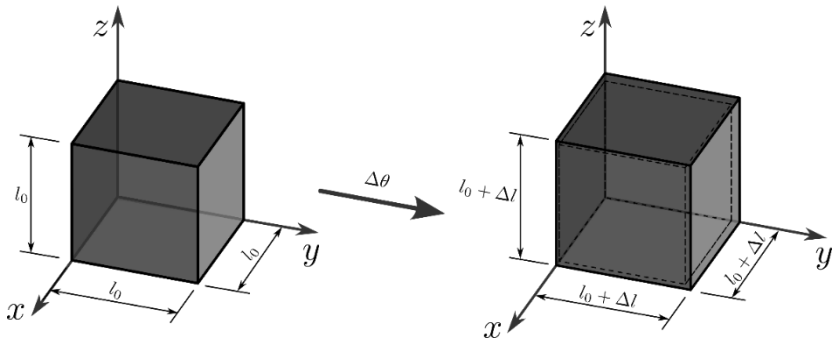


Figure 1. Thermoelastic cube subjected to uniform temperature change

In the second stage of a non-realistic analysis is used to test the non-annihilation of the material when subjected to large volumetric variations due to temperature. Thus, the thermoelastic response of the cube under large strains was evaluated, considering thermal contraction due to a temperature change of up to $\Delta\theta = -300$ K. The material properties adopted were: $E = 1$ Pa (Young's modulus), $\nu = 0$ (Poisson's ratio), and $\alpha_l = 0.01$ K^{-1}.

Figure 2 presents the results of J versus $|\Delta\theta|$ (Jacobian versus temperature change) for both constitutive models. These results are shown for comparison purposes only, since such a level of volumetric strain associated with this temperature change does not occur in practice. Nevertheless, they highlight the superior overall performance of the Rivlin-Saunders-Hartmann-Neff thermoelastic model compared to the Saint-Venant-Kirchhoff thermoelastic model.

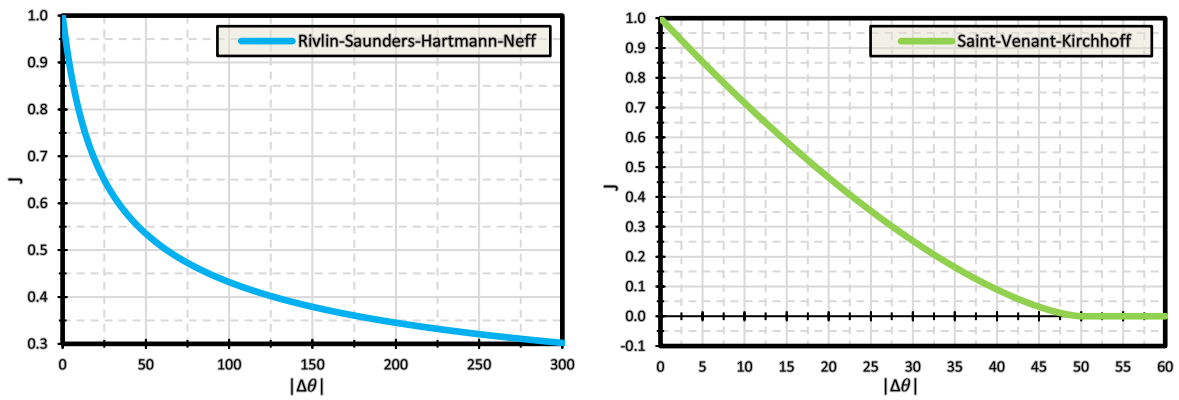


Figure 2. Plot of Jacobian versus temperature change

From the graph above, it can be observed that the thermoelastic model implemented using the Rivlin–Saunders–Hartmann–Neff formulation satisfies the growth condition, thus preventing material annihilation. In contrast, the Saint-Venant–Kirchhoff thermoelastic model exhibits a Jacobian determinant approaching zero at a temperature change of approximately $|\Delta\theta| = 50$ K, indicating that the material has lost its existence as a continuum body.

6 Numerical Example 2 – Thermoelastic beam

Originally analyzed by Zhang et al. [15], this numerical example concerns the quasi-static transient analysis of a thermoelastic cantilever beam subjected to a uniformly distributed transverse mechanical load of magnitude q (applied on the $y = 2$ cm face), a constant heat flux (applied on the $z = 8$ cm face), and convective heat transfer (on the $y = 2$ cm face). The beam has an initial uniform temperature of 293.15 K and a prescribed temperature of 298.15 K at the clamped end ($z = 0$ cm). The problem is illustrated in Fig. 3. Mechanical field data: $E = (90.06 + 0.3\theta)$GPa, $\nu = 0.3$, $q = (6250t)\text{N/m}^2$ (t in seconds). Thermal field data: $\alpha_l = 1.25 \cdot 10^{-5}\text{K}^{-1}$, $k = (21.34 + 0.05\theta)$ W/(m·K) (thermal conductivity), $c = 460$ J/(kg·K), $\rho = 7850$ kg/m^3, $\bar{q}_0 = 5000$ W/m^2, $h^c = 30$ W/(m^2·K), $\theta_\infty = 373.15$ K.

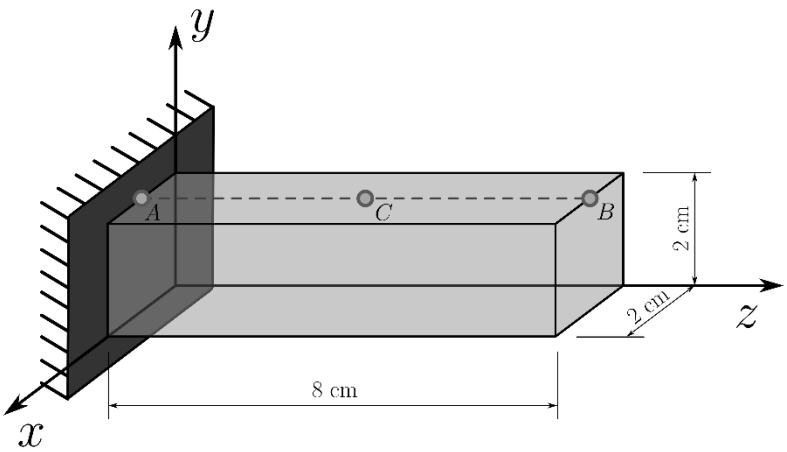


Figure 3. Initial configuration of thermoelastic cantilever beam

The results obtained were compared with those presented by Zhang et al. [15] and are organized into two graphs. The first graph shows temperature versus time, while the second presents absolute displacement versus time, as shown in Fig. 4.

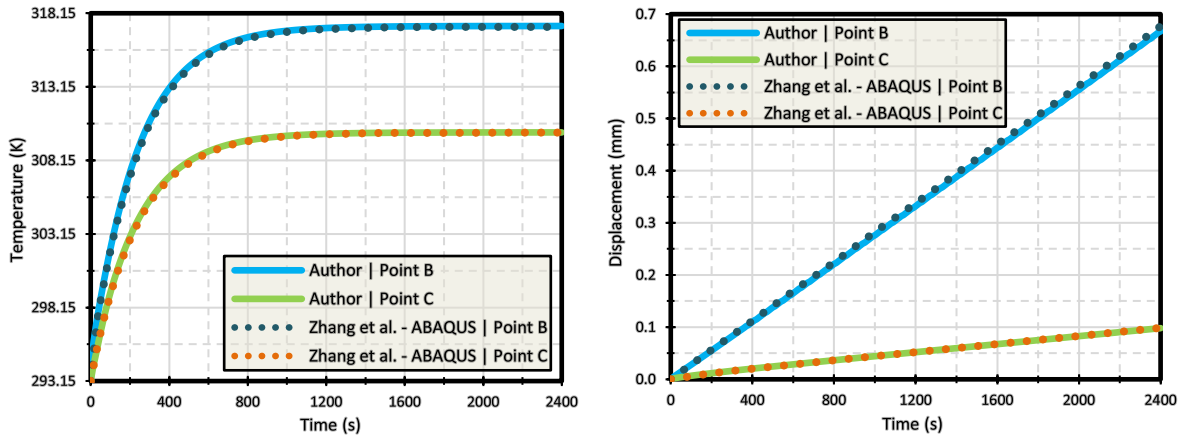


Figure 4. Plot of displacement versus time

7 Conclusions

This study presented an alternative thermoelastic model based on the Rivlin-Saunders and Hartmann-Neff hyperelastic constitutive formulations. The model was implemented in a proprietary computational code employing the position-based FEM for the mechanical field and temperature-based FEM for the thermal field. Thermomechanical coupling was performed using a partitioned explicit approach. Results for large strain regimes demonstrated the superiority of the Rivlin-Saunders–Hartmann-Neff model associated with the new strain-temperature coupling over the Saint-Venant–Kirchhoff model, as it satisfies the growth condition. The developed computational code was successfully validated against example from the scientific literature, confirming that the proposed formulation can satisfactorily simulate the thermoelastic behavior of structures subjected to thermal loads and temperature changes. An immediate future development is to solve the heat conduction considering current positions.

Acknowledgements. This work was supported by the Coordenação de Aperfeiçoamento de Pessoal de Nível Superior (CAPES) [Finance code 001], the Conselho Nacional de Desenvolvimento Científico e Tecnológico (CNPq) [Grant number 131185/2022-5] and the Fundação de Amparo à Pesquisa do Estado de São Paulo (FAPESP) [Grant number 2024/01594-6].

Authorship statement. The authors hereby confirm that they are the sole liable persons responsible for the authorship of this work, and that all material that has been herein included as part of the present paper is either the property (and authorship) of the authors, or has the permission of the owners to be included here.

References

[1]P. J. Flory, “Thermodynamic relations for high elastic materials”. *Transactions of the Faraday Society*, vol. 57, pp. 829–838, 1961.
[2]R. S. Rivlin and D. W. Saunders,“Large elastic deformations of isotropic materials VII. Experiments on the deformation of rubber”. Philosophical Transactions of the Royal Society of London, vol. 243, n. 865, pp. 251–288, 1951.
[3] S. Hartmann and P. Neff, “Polyconvexity of generalized polynomial-type hyperelastic strain energy functions for near-incompressibility”. *International Journal of Solids and Structures*, vol. 40, n. 11, pp. 2767–2791, 2003.
[4] E. Y. Hayashi. “Uma formulação baseada na decomposição de Flory para análise termomecânica de sólidos termo-visco-elasto-plásticos”. MSc thesis, São Carlos School of Engineering - University of São Paulo, 2024.
[5] H. B. Coda. “O método dos elementos finitos posicional: sólidos e estruturas - não linearidade geométrica e dinâmica”.EESC/USP, 2018.
[6] J. Bonet, R. Wood, J. Mahaney, and P. Heywood,“Finite element analysis of air supported membrane structures”. *Computer methods in applied mechanics and engineering*, vol. 190, n. 5-7, pp. 579–595, 2000.
[7] H. B. Coda. “Análise não linear geométrica de sólidos e estruturas: Uma formulação posicional baseada no MEF”. Thesis submitted as part of the Full Professor promotion process, São Carlos School of Engineering - University of São Paulo, 2003.
[8] É. S. Ramos, R. Carrazedo, and R. R. Paccola, “Modeling particles elements in damaged reinforced concrete structures”. *Latin American Journal of Solids and Structures*, vol. 18, pp. e345, 2021.
[9] V. H. Kishino, R. T. Kishino and H. B. Coda,“A sequential investigation of the residual stresses and strains influence on the buckling of cold-formed thin-walled members”. *Thin-Walled Structures*, vol. 180, pp. 109814, 2022.
[10] P. R. P. Carvalho, H. B. Coda and R. A. K. Sanches,“A large strain thermodynamically-based viscoelastic–viscoplastic model with application to finite element analysis of polytetrafluoroethylene (PTFE)”. *European Journal of Mechanics - A/Solids*, vol. 97, pp. 104850, 2023.
[11]R. De Borst, M. A. Crisfield, J. J. Remmers, and C. V. Verhoosel. “Nonlinear finite element analysis of solids and structures”. John Wiley & Sons, 2012.
[12] R. Rigobello, H. B. Coda, J. Munaiar Neto. “A 3D solid-like frame finite element applied to steel structures under high temperatures”. *Finite Elements in Analysis and Design*, vol. 91, pp. 68-83, 2014.
[13] R. C. Salomão, R. Carrazedo, “Thermal conduction modeling of composites by embedding technique”. *Proceedings of the Institution of Mechanical Engineers, Part L: Journal of Materials: Design and Applications*, vol. 236, n. 7, pp. 1443–1453, 2022.
[14] V. H. Kishino. “Estabilidade de elementos estruturais de parede fina após conformação a frio: uma estratégia elasto-plástica baseada na decomposição de Flory”. MSc thesis, São Carlos School of Engineering - University of São Paulo, 2022.
[15] S. Zhang, Y. Cai, H. Wang, E. Li, G. Li and Y. Wu,“A fast reanalysis solver for 3D transient thermo-mechanical problems with temperature-dependent materials”. *Computers & Structures*, vol. 238, pp. 106298, 2020.